PAPER 10 (SESSION I)

Stress distribution and buckling in thin sheets with central slits

J. R. DIXON and J. S. STRANNIGAN
National Engineering Laboratory, East Kilbride, Glasgow.

Summary
Measurements were made of buckling deformation and associated stress fields around central slits in photoelastic models and metal sheets under a tensile load. The maximum stress at the tip of the slit increased, as buckling developed, above that obtained with buckling restrained. The results are discussed in relation to the effect of buckling on the static strength and fatigue crack growth characteristics of centrally cracked sheets. The critical load for onset of buckling could be estimated using a modified Buler formula for a straight bar under end load.

Introduction

The tangential stress σ_c at the boundary of a central crack in a uniaxially loaded sheet under tension is compressive along most of the boundary, hence crack buckling can occur in thin sheets. It is well known that buckling can affect the fracture characteristics of sheet-like structures.

Analytical solutions of stresses around cracks, when buckling has occurred, are virtually non-existent. Some progress in this field has been made by Cherepanov [1], but the assumptions in his mathematical model are rather restrictive and do not cover the problem of a central crack in a uniaxially loaded sheet. This paper describes the measurement of buckling deformation and associated stress fields around central slits in photoelastic models and metal sheets. The results are discussed in relation to the static strength and fatigue crack growth characteristics of cracked sheets when crack buckling is present.

Compressive stress field around a crack

Let σ_p and σ_q be the principal stresses in an infinite sheet containing a central crack of length 21 and subjected to an applied tensile stress σ normal to the line of the crack (Fig. 1). Except in the vicinity of the crack tip, the directions of σ_p and σ_q are roughly parallel to the x and y axes respectively, The stress σ_q is always tensile but σ_p can be either tensile or compressive. Contours of constant σ_p/σ, obtained from the theoretical elastic solution for an infinite sheet [2, 3] and showing the region around the crack where σ_p is compressive, are plotted in

Fig. 2. Although the region where $\sigma_p < 0$ is extensive, the higher values of compressive σ_p, for example, $\sigma_p < -0{\cdot}3\sigma$, occur in a comparatively small region, approximately within $|x/l| < 1{\cdot}0$, $|y/l| < 0{\cdot}5$.

On the y-axis, $\sigma_p = 0$ at E (Fig. 1) where $y = e$ and $\sigma_q - \sigma_p$ has a relative minimum value at D where $y = d$. The theoretical elastic solution for an infinite sheet gives $e/l = 0{\cdot}79$ and $d/l = 0{\cdot}71$.

Stress and buckling measurements on photoelastic models

Photoelastic models, Nos A1-A3, were machined from sheets of Araldite CT200 to the geometry of Fig. 3; detailed dimensions are given in Table 1. Each model was loaded axially through metal plates bolted to the ends, tests were carried out at room temperature and the stress distribution obtained by normal two-dimensional photoelastic techniques. Models A1 and A2 were used to study the variations of d/l and σ_c/σ with slit-length/sheet-width ratio l/b; no buckling occurred in these models. Model A3 was used to study the variation of σ_c/σ, σ_{max}/σ and δ with σ for (a) buckling and (b) with buckling restrained, where σ_{max} is the maximum stress which occurs at the ends of the slit and δ the out-of-plane deflection of the lip of the slit due to buckling. All stress measurements were averaged through the thickness of the sheet. Three modes of buckling were observed and are sketched in Fig. 4; mode 1 was the most common. A photograph of model A3 in buckling mode III is shown in Fig. 5.

The variation of d/l with l/b (Fig. 6), for no buckling, shows that the experimental value of d/l tends to the theoretical infinite sheet value of 0·71 as l/b tends to zero. Generally d/l increases with l/b, indicating that the region on either side of the slit, subject to high compressive stresses, is larger for finite l/b than for a sheet of infinite width ($l/b = 0$). The value of $(-\sigma_c/\sigma)$ also generally increases as l/b increases (Fig. 7), for no buckling, σ_c/σ tending to the theoretical infinite sheet value of -1 as l/b tends to zero.

The variations of σ_{max}/σ, σ_c/σ and δ/l with σ/E in model A3 for unrestrained buckling are plotted in Fig. 8. The tests on model A3 were repeated with buckling restrained by steel plates covering the model (small holes were drilled in the plates so that photoelastic measurements could be made near the slit in the model); the plates were greased to reduce frictional effects. The results are included in Fig. 8.

With no restraint, buckling occurred as soon as load was applied and δ and σ_{max}/σ increased with σ, whereas with buckling restrained $\delta = 0$ and σ_{max}/σ remained constant. The variation of a factor C, where

$$(\sigma_{max}/\sigma)\ \text{buckling unrestrained} = C \times (\sigma_{max}/\sigma)\ \text{buckling restrained},$$

with δ/l in Fig. 9 was obtained by replotting the results of Fig. 8. An approximation to the experimental $(C, \delta/l)$ curve is given by

$$C = 1 + 20\left(\frac{\delta}{l}\right)^2.$$

Dixon [4] has shown that σ_{max}/σ for no buckling can be expressed by

$$\frac{\sigma_{max}}{\sigma} = \left\{1 + 2\left(\frac{l}{\rho}\right)^{1/2}\right\}\left\{1 - \left(\frac{l}{b}\right)^2\right\}^{-1/2}$$

Substituting the values of l, ρ and b for model A3 from Table 1 gives $\sigma_{max}/\sigma = 15{\cdot}8$, which agrees well with the measured restrained value. The restrained value of $(-\sigma_c/\sigma)$ were slightly lower than the corresponding value from the thicker models A1 and A2 (Fig. 7); this may have been due to the buckling restraint on model A3 not being perfect. The unrestrained value of $(-\sigma_c/\sigma)$ for buckling mode I, this was the natural buckling mode for model A3, decreased with increasing σ; the effect of buckling would tend to limit the value of σ_c. Buckling modes II and III could be easily obtained by applying a slight transverse pressure by hand to the appropriate lip of the slit.

Tests were also carried out on sheet photoelastic models with central slits having a reflecting surface in the mid-plane of the sheet, and on aluminium-alloy sheets with central slits having coatings of photoelastic material bonded to each side of the sheet around the slits. By reflecting polarized light from the reflecting surface inside the model, or from the surfaces of the metal sheet, it was possible, using photoelastic reflection techniques, to obtain an indication of stress variation through the sheet thickness. Accurate measurement of peak stresses in the above types of specimen proved difficult but there was no indication that any great variation of maximum stress at the end of the slit through the sheet thickness occurred with buckling. This was not unexpected as the ends of the slit were near to points of inflexion on the buckling contour of the sheet (see Fig. 4) and bending stresses through the thickness of the sheet in these regions would be small.

Buckling measurements on aluminium-alloy specimens

Tensile specimens with central slits were machined from aluminium-alloy sheets of thickness (t) 0·94 and 2·01 mm (0·037 and 0·079 in) to dimensions given in Fig. 10 and Table 2. Mechanical properties of the materials are also included in Table 2. Each specimen was loaded in tension through plates bolted to the ends.

Specimens D1-D4 were used to determine the critical applied stress for buckling for various slit lengths. Strain gauges were attached near a lip

of the slit on both sides of the sheet (Fig. 10) and strain readings ϵ_1 and ϵ_2, for sides 1 and 2 respectively, were taken as the load on the specimen was increased. The strain difference $\Delta\epsilon = \epsilon_1 - \epsilon_2$ gave a measure of buckling and a typical $(\Delta\epsilon, \sigma/E)$ plot is drawn in Fig. 11. Buckling was said to occur at $\sigma = \sigma_{crit}$ when $\Delta\epsilon$ commenced to change rapidly with σ. However, the value of σ_{crit} could not be determined precisely and upper and lower limits of σ_{crit} were obtained as shown in Fig. 11. The variation of σ_{crit} with l/b is plotted in Figs. 12 and 13 for $t = 0{\cdot}94$ mm (0·037 in) and 2·01 mm (0·079 in) respectively. Values of σ_{crit} from specimens D5 and D6 for $l/b = 0{\cdot}3$ are also included in Fig. 12.

Specimens D5 and D6 with $l/b = 0{\cdot}3$ were loaded until fast fracture of the sheet occurred; δ was measured during loading. Values of δ/l are plotted against σ/E in Fig. 14. Tests were repeated with specimens D7 and D8 but with buckling restrained by steel bars greased to reduce frictional effects and lightly clamped across the slit in the direction of the load. In all cases, a little slow cracking occurred initially at the tip of the slit followed by fast fracture across the rest of the section. Table 3 lists the values of σ and δ at the point of fast fracture and it can be seen that buckling slightly reduced the static strength of the sheets.

Theoretical estimate of σ_{crit}

As an approximately transverse compressive stress σ_p exists near the lips of the slit or crack, with $\sigma_p = \sigma_c$ at the lip, the theory of buckling of centrally compressed bars suggests that buckling will commence when

$$\sigma_c = \frac{\lambda E t^2}{l^2} \tag{1}$$

where λ is a constant for a given crack configuration.

If the critical region of compressive stress on either side of the crack is considered to be a rectangular bar of length $2l_e$ with a uniform compressive stress σ_c applied at its ends (Fig. 15), Euler's formula for hinged ends [5] gives $\lambda = \pi^2/48$. If it is assumed that $\sigma_c = -\sigma$ for all l/b and $\sigma = \sigma_{crit}$ at the onset of buckling, then equation (1) becomes,

$$\sigma_{crit} = \frac{\pi^2 E t^2}{48\, l_e^{\,2}} \tag{2}$$

Substituting values of $l_e = 0{\cdot}4l$ and $0{\cdot}6l$ in equation (2) gives reasonable agreements with the experimental values of σ_{crit} for the aluminium-alloy specimens for $t = 0{\cdot}94$ mm (0·037 in) (Fig. 12) and $t = 2{\cdot}01$ mm (0·079 in) (Fig. 13) respectively. Strictly, $\sigma_c \neq \sigma$ for $l/b > 0{\cdot}6$ approximately, and if equation (2) were modified to take into account the

(σ_c, σ) relationship from Fig. 7, better agreement between the experimental and theoretical values of σ_{crit} would be obtained for the higher l/b ratios.

Relationships similar to equation (2) have also been used successfully by Liu [6] and Forman [7] to predict the onset of buckling in centrally cracked aluminium-alloy sheets for $t = 2{\cdot}01$ mm (0·079 in) and 1·52 mm (0·060 in). They assumed $\sigma_c = \sigma_{net}$ as opposed to $\sigma_c = \sigma$ in the present work, but Fig. 7 shows the latter expression to be physically more realistic, at least for $l/b < 0{\cdot}6$. Clarkson [8] found that an expression $\sigma_{crit} = 1{\cdot}18\,E\,(t/l)^2$ fitted experimental results from centrally-cracked aluminium-alloy sheets of $t = 1{\cdot}63$ mm (0·064 in) and 0·25 m (10 in) wide; equation (2) gives $\sigma_{crit} = 1{\cdot}28\,E\,(t/l)^2$ and $0{\cdot}57\,E\,(t/l)^2$ for $t = 0{\cdot}94$ mm (0·037 in) and 2·01 mm (0·079 in) respectively. Walker [9] in a parametric study of buckling behaviour showed a reasonable correlation of results from 0·51 m (20 in) wide aluminium-alloy sheets of thickness varying between 0·81 and 2·03 mm (0·032 and 0·080 in) and from 0·30 m (12 in) wide sheets of titanium of thickness 0·51 and 1·14 mm (0·020 and 0·045 in), by plotting $\sigma_c/(Et^2)^{1/2}$ against $l/(Et^2)^{1/4}$. The present results show a fair correlation if plotted in this manner.

Discussion

The photoelastic results in Fig. 8 show that the maximum stress σ_{max} at the tip of the slit in the unrestrained model was about thirty per cent greater than the corresponding value when buckling was restrained, for $t = 0{\cdot}43$ mm (0·017 in), $l = 0{\cdot}063$ m (2·5 in), $b = 0{\cdot}13$ m (5 in), $\sigma/E = 0{\cdot}0025$ and $\delta/l = 0{\cdot}12$. Unstable fracture of the two aluminium-alloy specimens D5 and D6 (Fig. 14), with $t = 0{\cdot}94$ mm (0·037 in) and $l = 0{\cdot}076$ m (3 in) occurred at approximately $\sigma/E = 0{\cdot}0025$ and $\delta/l = 0{\cdot}12$. The static strength of these two specimens was on average about ten per cent lower than when buckling was restrained (Table 3). This decrease in strength is less than might have been expected on the basis of the photoelastic results, but nominal stresses across the cracked section of specimens D5-D8 were of the order of the 0·1 per cent proof stress of the material and plastic deformation would be expected to modify significantly the elastic stress and strain distributions in the region of the crack tip and hence influence the static strength. Similar reductions in static strength due to crack buckling in various aluminium-alloy sheets of thickness ranging from 0·81-2·03 mm (0·032-0·080 in) were measured by Walker [9] and Trotman [10]. However, Forman [7] found that crack buckling in AM355CRT steel sheet, tensile yield stress = 1·53 GN/m² (222 400 lb/in²), caused a reduction in static strength up to forty per cent for $t = 0{\cdot}51$ mm (0·020 in) and $l = 0{\cdot}13$ m

(5 in) with $\sigma/E = 0{\cdot}0016$. In this case the nominal stress across the cracked section at unstable fracture was about 0·4 times the yield stress of the material.

Kuhn [11], in an analysis of notch and crack strength under static and fatigue loadings quotes results of tests on 2024-T3 aluminium-alloy sheet, $l = 0{\cdot}22$ m (8·5 in) and $b = 0{\cdot}44$ m (17·5 in), showing a twenty-five per cent reduction in static strength when buckling was unrestrained compared to a restrained sheet. He also suggested that the stress concentration factor for a uniaxially loaded sheet containing a central slit should be increased by a factor B,

$$B = \left(1 - 0{\cdot}001\frac{2l}{t}\right)^{-1}, \tag{3}$$

to allow for buckling, but points out that this factor is not well substantiated. Equation (3) does not take into account any effect due to the amount of buckling (δ) which will vary with the applied stress. Putting $2l = 0{\cdot}064$ m (2·5 in) $t = 0{\cdot}43$ mm (0·017 in), from the photoelastic model A3, into equation (3) gives $B = 1{\cdot}17$, that is a seventeen per cent increase in the stress concentration factor. This increase is about in the middle of the range zero to thirty per cent for the photoelastic model, as shown by the (C, δ/l) curve in Fig. 9; thus it would appear that equation (3) could give correction factors of the right order. Cricklow and Wells [12] used $1/B$ as a correction factor to allow for the effect of buckling on the static strength of cracked titanium and aluminium-alloy sheets.

The stress intensity factor K is related to the magnitude of the elastic stress field in the immediate vicinity of the crack, and for a uniaxially loaded sheet with a central crack

$$K = \alpha\sigma l^{1/2} \tag{4}$$

where α is a constant depending on the geometry of the sheet. Alternatively K can be derived from [13]

$$K = \lim_{\rho \to 0} \tfrac{1}{2}\sigma(\pi\rho)^{1/2}\frac{\sigma_{\max}}{\sigma} \tag{5}$$

where the general relationship between $\sigma_{\max}/\sigma$ and ρ is known analytically. The photoelastic results of Fig. 9 show that $\sigma_{\max}/\sigma$ can increase considerably due to crack buckling, and according to equation (5) such an increase for a sharp crack would have a significant effect on the corresponding K. Thus, any elevation of the stress field near the crack

tip caused by buckling would necessitate modifications to the right-hand side of equations (4) and (5) to enable K to be calculated correctly. A semi-empirical analysis of unstable crack propagation is given by Welbourne [14] who uses an effective crack tip strain concentration factor as a criterion for instability. This strain concentration factor will, of course, be affected by crack buckling and again this should be taken into account in the analysis if buckling occurs in the test specimen. In general, it would be very difficult to allow for buckling in an accurate analysis of test results; thus in practice, for material evaluation as for example in fracture toughness testing, buckling should be eliminated and so the possibilities of large errors due to this avoided.

Frost [15] has shown experimentally that the rate of growth of fatigue cracks in uniaxially loaded metal sheets, when the nominal stresses in the sheet are below the yield stress of the material, obeys the relationship

$$\frac{dl}{dn} = A\sigma_a^m\, l \tag{6}$$

where A is a material constant which may or may not depend on the mean stress, σ_a the semi-range of the applied stress and m has a value between 2 and 3. Frost and Dixon [16] have also shown theoretically that crack growth laws of the type given in equation (6) follow from an analysis of the changing crack tip profile during the loading and unloading cycle. The crack tip profile can be related to the strain concentration at the tip. Fatigue crack growth rates can also be correlated with a stress intensity factor K, for example [17]

$$\frac{dl}{dn} = MK^4$$

where M is a constant. As shown, buckling can increase the magnitude of the stress and strain field at a crack tip and hence one would expect it to cause an increase in the rate of growth of a fatigue crack in a thin sheet. Cricklow and Wells [12] showed that the crack growth rate in titanium panels {dl/dn of the order of 10^{-3} in per cycle, $l \simeq 0{\cdot}064$ m (2·5 in)} was ten times faster with buckling present than when buckling was restrained. Rooke and others [18] found that buckling had very little effect on the rate of growth of fatigue cracks in a sheet aluminium alloy of thickness 1·63 mm (0·064 in). However, for the stresses applied, it would appear that the maximum value of δ/l in these tests was less than 0·05 and the increase in stress near the crack tip due to buckling may well have been small. For example, Fig. 9 shows an increase in $\sigma_{\max}$ due to buckling of only eight per cent for $\delta/l = 0{\cdot}05$. Crack

buckling has also a significant effect on the growth of fatigue cracks in sheets under a static tensile load and subjected to a superimposed acoustic loading [8]. The stress fields in the latter are, of course, more complex than the ones considered here.

Acknowledgments

This paper is published by permission of the Director of the National Engineering Laboratory, Ministry of Technology. It is Crown copyright and is reproduced by permission of the Controller of H.M. Stationery Office.

Notation

B, C	Factors
$2b$	Sheet width
d, e	Distances along y-axis
E	Young's modulus
$2l$	Crack (slit) length
$2l_e$	Effective crack length in buckling
n	Number of cycles
t	Sheet thickness
x, y	Cartesian coordinates
Y	0·1 per cent proof stress
Δ_ϵ	Strain difference
δ	Out-of-plane deflection of lip of slit
ϵ_1, ϵ_2	Strain
ρ	Radius at tip of slit
σ	Nominal stress on gross section
σ_c	Tangential stress along lip of crack (slit)
σ_{crit}	Critical buckling stress
σ_{max}	Maximum stress at end of slit
σ_{net}	Nominal stress on net section
σ_p, σ_q	Principal stresses

denotes value at unstable fracture

References

1. CHEREPANOV, G. P. 'On the buckling under tension of a membrane containing holes'. *J. appl. Maths. Mech., PMM*, vol. 27(2), pp. 405-420, 1963.
2. INGLIS, C. E. 'Stresses in a plate due to the presence of cracks and sharp corners'. *Trans. Instn. nav. Archt.*, vol. 55(1), pp. 219-239, 1913.
3. DIXON, J. R. 'Computed values of the elastic stresses around a crack in an infinite plate under tension'. *NEL Report* No. 12. East Kilbride, Glasgow: National Engineering Laboratory, 1961.

4. DIXON, J. R. 'Stress distribution around a central crack in a plate loaded in tension; effect of finite width of plate'. *Jl. R. aeronaut. Soc.*, vol. 64(591), pp. 141-145, 1960.
5. TIMOSHENKO, S. *Theory of elastic stability*. New York: McGraw-Hill, 1936.
6. LIU, H. W. Discussion, *Proc. Crack Propagation Symposium, Cranfield*, September 1961, vol. 2, pp. 514-526. Cranfield: College of Aeronautics, 1962.
7. FORMAN, R. G. 'Experimental program to determine effect of crack buckling and specimen dimensions on fracture toughness of thin sheet materials'. *Report No.* AFFDL-TR-146. Ohio: Air Force Flight Dynamics Laboratory, 1966.
8. CLARKSON, B. L. 'The propagation of fatigue cracks in a tensioned plate subjected to acoustic loads'. *In* Trapp, W. J. and Forney, D. (Eds.) *Acoustical fatigue in aerospace structures*, pp. 361-388. Syracuse, N.Y.: Syracuse University Press, 1965.
9. WALKER, E. K. 'A study of the influence of geometry on the strength of fatigue-cracked panels. *Report No.* AFFDL-TR-66-92. Ohio: Air Force Flight Dynamics Laboratory, 1966.
10. TROTMAN, C. K. Discussion; *Proc. Crack Propagation Symposium, Cranfield*, vol. 2, pp. 538-539. Cranfield: College of Aeronautics, 1962.
11. KUHN, P. 'The prediction of notch and crack strength under static or fatigue loading'. Air Transport and Space Meeting. *ASTM(SAE) Paper No.* 843C. New York: American Society for Testing Materials, 1964.
12. CRICKLOW, W. J. and WELLS, R. H. 'Crack propagation and residual static strength of fatigue-cracked titanium and steel cylinders'. Fatigue crack propagation. *ASTM STP* 415. New York: American Society for Testing Materials, 1967.
13. IRWIN, G. R. 'Fracture mechanics'. *In* Goodier, J. N. and Hoff, N. J. (Eds.) *Structural mechanics*, pp. 557-591. Oxford: Pergamon, 1960.
14. WELBOURNE, E. R. 'The correlation of unstable crack length data for sheet materials'. *Aeronaut. Q.*, vol. 12, pp. 395-408, 1961.
15. FROST, N. E. 'The growth of fatigue cracks'. Proc. 1st Int. Conf. Fracture, Sendai, Japan, pp. 1433-1459, 1965.
16. FROST, N. E. and DIXON, J. R. 'A theory of fatigue-crack growth'. *Int. J. fracture Mech.*, vol. 3(4), pp. 301-316, 1967.
17. PARIS, P. and ERDOGAN, F. 'A critical analysis of crack propagation laws'. *J. bas. Engng*, vol. 85, pp. 528-534, 1963.
18. ROOKE, D. P., GUNN, N. J. F., BALLET, J. T. and BRADSHAW, F. J. 'Crack propagation in fatigue. Some experiments with DTD 5070A aluminium sheet'. *Tech. Report* No. 64025. Farnborough: Royal Aircraft Establishment, 1964.

Table 1

Details of photoelastic models

Model No	2h m (in)	2b m (in)	2l m (in)	ρ mm (in)	t mm (in)	Test measurements
A1	0·20 (8)	0·10 (4)	0·025-0·097 (1·0-3·8)	0·79 (0·031)	1·58 (0·062)	$\frac{d}{l}, \frac{\sigma_c}{\sigma} v \frac{l}{b}$ no buckling
A2	0·20 (8)	0·10 (4)	0·013-0·091 (0·5-3·6)	0·079 (0·031)	1·50 (0·059)	
A3	0·25 (10)	0·13 (5)	0·064 (2·5)	0·079 (0·031)	0·43 (0·017)	$\frac{\sigma_c}{\sigma}, \delta, \frac{\sigma_{max}}{\sigma} v \sigma$ with (a) buckling (b) buckling restrained

Table 2

Details of aluminium-alloy specimens

Specimen No.	0·1% Proof stress MN/m² (lb/in²)	Tensile strength MN/m² (lb/in²)	E GN/m² (lb/in²)	2b m (in)	2l m (in)	ρ mm (in)	t mm (in)	Test measurements
D1, D2	309 (44 800)	414 (60 000)	68·9 (10 × 10⁶)	0·25 (10)	0·038-0·228 (1·5-9·0); 0·062-0·114 (2·5-4·5)	0·79 (0·031)	0·94 (0·037)	$\Delta\epsilon$ v σ
D3, D4	215 (31 200)	255 (37 000)	75·8 (11 × 10⁶)	0·25 (10)	0·038-0·218 (1·5-8·6); 0·062-0·114 (2·5-4·5)	0·79 (0·031)	2·01 (0·079)	σ_{crit}
D5-D8	269 (39 000)	303 (43 900)	68·9 (10 × 10⁶)	0·25 (10)	0·076 (3·0)	0·79 (0·031)	0·94 (0·037)	δ v $\frac{\sigma}{\sigma'}$

′ denotes value at unstable fracture

Table 3

Static strength of sheets with central slit

Specimen No	σ' MN/m² (lb/in²)	σ'_{net} MN/m² (lb/in²)	$\frac{\sigma'_{net}}{Y}$	$\frac{\delta'}{l}$	
D5	170 (24 600)	238 (34 500)	0·88	0·10	Buckling
D6	178 (25 800)	253 (36 700)	0·94	0·14	Buckling
D7	187 (27 200)	268 (38 900)	1·00	0	Buckling restrained
D8	187 (27 200)	268 (38 900)	1·00	0	Buckling restrained

′ denotes value at unstable fracture

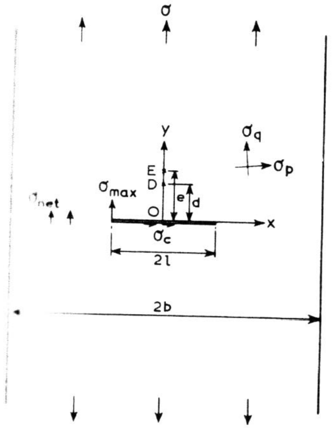

Fig. 1. Notation.

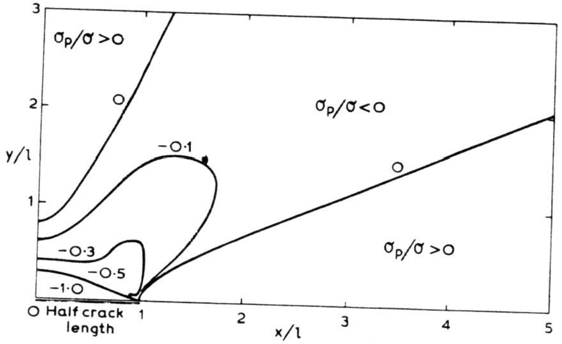

Fig. 2. Contours of σ_p/σ.

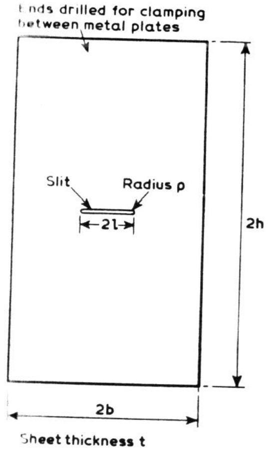

Fig. 3. Photoelastic model.

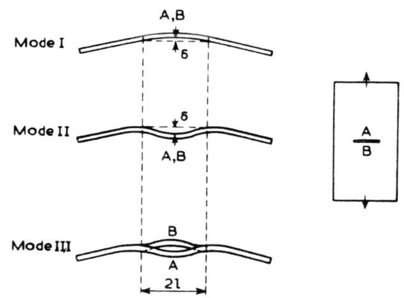

Fig. 4. Modes of buckling.

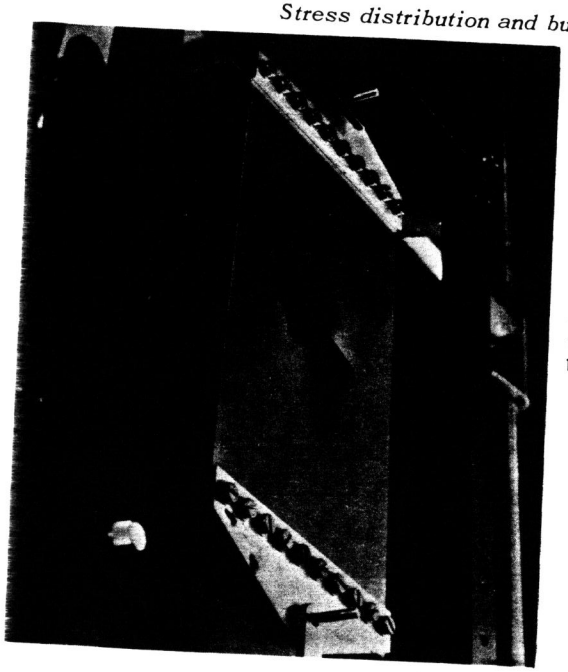

Fig. 5. Photoelastic model under axial tensile load; buckling mode III.

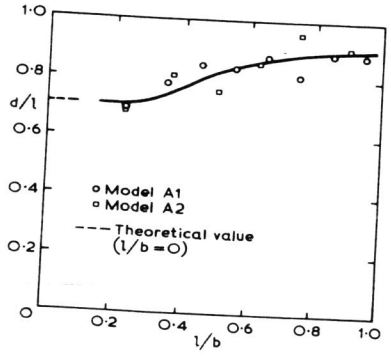

Fig. 6. Photoelastic model; variation of d/l with l/b, no buckling.

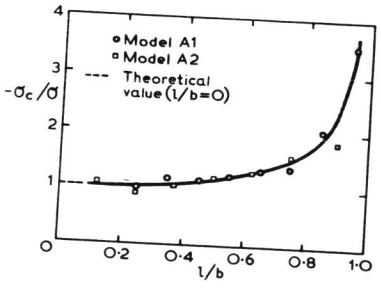

Fig. 7. Photoelastic model; variation of σ_c/σ with l/b, no buckling.

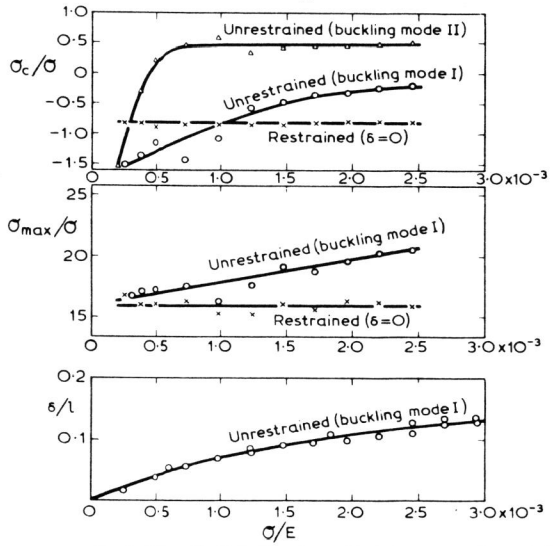

Fig. 8. Photoelastic model; variation of σ_{max}/σ, σ_c/σ and δ/l with σ/E.

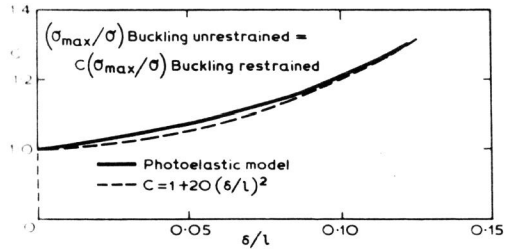

Fig. 9. Variation of C with δ/l.

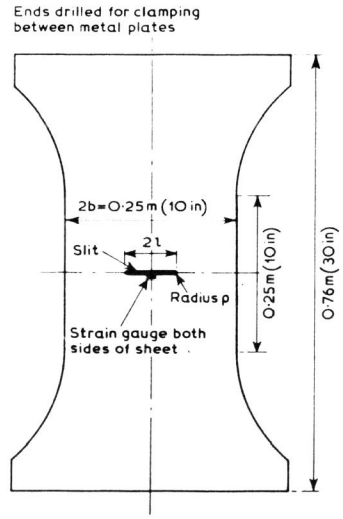

Fig. 10. Aluminium alloy specimen.

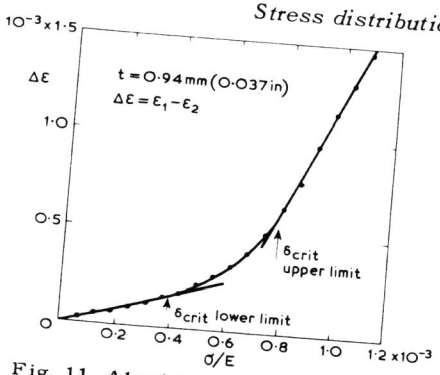

Fig. 11. Aluminium alloy specimen D1, $\Delta\epsilon$v σ/E for $l/b = 0{\cdot}35$.

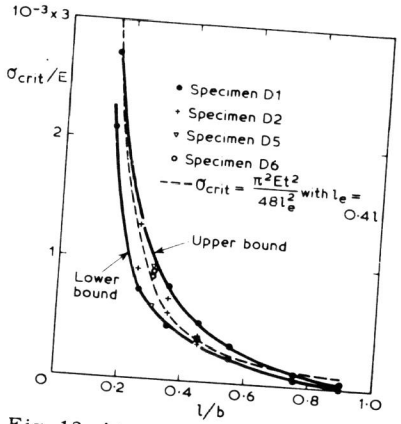

Fig. 12. Aluminium alloy; variation of critical buckling stress with l/b, t = 0·94 mm. (0·037 in).

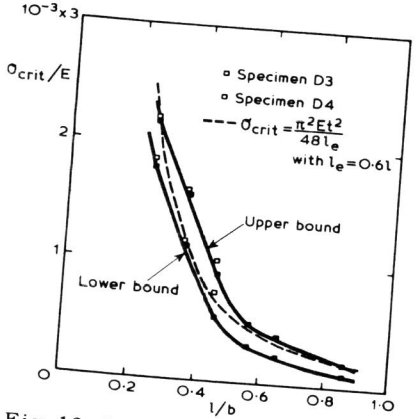

Fig. 13. Aluminium alloy; variation of critical buckling stress with l/b, t = 2;01 mm. (0·079 in).

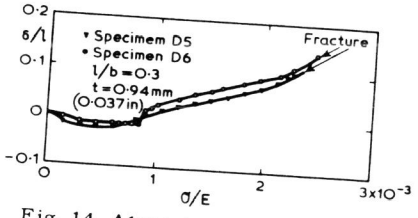

Fig. 14. Aluminium alloy; buckling deflection.

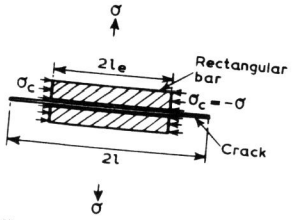

Fig. 15. Crack buckling; mathematical model.